Turbulent Boundary-Layer Diffusion Flame: Effects of Probability Density Function

Chiun-Hsun Chen,* Chern-Yang Lan,*
National Chiao-Tung University, HsinChu, Taiwan, 30050 Republic of China
and
David Y. Shan†
Chung Shan Institute of Science and Technology, LungTan, Taiwan, 32525 Republic of China

A turbulent diffusion flame adjacent to a solid fuel in a parallel airflow is studied analytically. The flow is assumed to be of boundary-layer type where the mean properties of flowfield are predicted by a low-Reynolds-number K-ϵ two-equation model. The chemical reaction is approximated as one-step and infinite-fast. The mean mass-fraction distribution in the boundary layer is described by probability density function (p.d.f.). Four kinds of p.d.f.s are used and they are beta, clipped Gaussian, double delta, and ten-point delta p.d.f.s respectively. The general features of each flame structure by applying corresponding p.d.f.s are quite similar. An overlap exists between fuel and oxidizer mean mass-fraction distributions. The maximal flame temperature is below the value of adiabatic one and its profile is rounded. The velocity, mixture fraction and its fluctuation, and total enthalpy are found to be almost invariant with the form of p.d.f.s. The mass fraction and temperature profiles appear nearly identical by the uses of beta and clipped Gaussian p.d.f.s. In application of double delta p.d.f., discontinuity shows up in these profiles. The modified ten-point delta p.d.f. has the maximum flame temperature due to its smallest overlap of $\bar{Y}_F$ and $\bar{Y}_O$ among these p.d.f.s.

Nomenclature

C_1, C_2 = constants
C_{g1}, C_{g2} = constants
C_f = skin-friction coefficient, $\tau_w/\left(\frac{1}{2}\rho u_\infty^2\right)$
C_p = average specific heat
C_μ = constant
D = species diffusivity
K = turbulent kinetic energy, $\frac{1}{2}(\overline{u_i' u_j'})$
K^* = nondimensional turbulent kinetic energy, K/u_∞^2
L_e = Lewis number, α/D
L_t = turbulent Lewis number
M = average molecular weight
P_r = Prandtl number
P_t = turbulent Prandtl number
T = temperature
u = velocity parallel to fuel surface
v = velocity normal to fuel surface
Y_F = fuel mass fraction
Y_O = oxidizer mass fraction
y^+ = dimensionless distance, $y^+ = \rho_w \tau_w y/\mu_w$
$\overline{(\ )}$ = time-averaged quantity
δ_0 = initial boundary-layer thickness
δ = 1) boundary-layer thickness. 2) δ-function
μ = 1) molecular viscosity. 2) mean value [Eqs. (2-19)]
μ_t = turbulent viscosity
σ_k, σ_ϵ = constants
σ = standard deviation
ρ = density
ϵ = turbulent energy dissipation rate, $\nu \cdot \overline{\frac{\partial u_i'}{\partial y}} \cdot \overline{\frac{\partial u_i'}{\partial y}}$
ϵ^* = nondimensional turbulent energy dissipation rate, $\frac{\epsilon}{u_\infty^4/\nu_\infty}$
τ = shear stress
τ^* = nondimensional shear stress, $\frac{\tau}{\rho_\infty u_\infty^2}$
ν = kinetic viscosity
$\dot{\omega}_i$ = species consumption rate per unit time per unit volume in gas phase

Subscripts
w = fuel surface
∞ = freestream
st = stoichiometric state
t = turbulent state

Superscript
$(\ )'$ = fluctuation quantity

Introduction

A TURBULENT boundary-layer combustion for a flame adjacent to a solid fuel placed in a parallel oxidizer flow is studied analytically. This is one of the fundamental problems for combustion science. Applications can extend to investigate the fire growth in the situation of wall fire as well as the burning rate and combustion efficiency of solid fuel in the combustor of the solid-fuel ramjet under special circumstance, etc.

The study of solid fuel turbulent reacting flow has proceeded for last two decades. Maxman employed the finite but thin-flame-sheet approximation leading to a modified Reynolds analogy to analyze the hybrid rocket combustion problem in which the freestream conditions changed with the streamwise distance.[1] The results indicate that the heat transfer and burning rates are in good agreement with that by the experimental works. Wooldridge and Muzzy performed the

Received Oct. 2, 1989; revision received Feb. 21, 1990.
*Department of Mechanical Engineering.
†Unavailable.

combustion experiment for a turbulent boundary flow with uniform wall injection of a hydrogen-nitrogen mixture as the fuel in the wind tunnel.[2] It shows that the flame zone occupies 10% of the total boundary-layer thickness, and the nondimensional measured velocity, enthalpy, and concentration profiles are found to be similar. This confirms the generalized Reynolds analogy is valid. Netzer and his colleagues adopted a K-ϵ two-equation model with a one-step infinite-fast chemical kinetics to study the solid-fuel ramjet combustion.[3] The flame structure predicted by use of thin-flame sheet theory, implying that there is no overlap between the time-averaged fuel and oxidizer-concentration distributions, is in contradiction to the experimental observation.[4] The work by Most et al.[5] was to study the influence of turbulence on heat transfer to a reactive wall in a square channel. The diffusion flame is obtained by injecting a gaseous fuel through a porous wall into the turbulent main airstream. The low-Reynolds-number K-ϵ model proposed by Jones and Launder is used.[6,7] The combustion is modified from mixing-layer formulation using instantaneous chemical equilibrium and clipped rectangle probability density function for the mixture fraction. It is found that mean temperature and velocity profiles, heat flux to the wall, and mass burning rate show good agreement with the experimental measurements. Recently, Shan and T'ien investigated the turbulent combustion boundary layer adjacent to a pyrolyzing solid fuel surface.[8] They adopted the low-Reynolds-number K-ϵ model as well to predict the mean properties of turbulent flowfield. The instantaneous thin-flame-sheet theory together with the beta probability density function for the mixture fraction were used for combustion model. The results show that the mean temperature profile is rounded with the maximum temperature well below the adiabatic value, and the time-averaged mass fraction distributions of fuel and oxidizer overlap substantially.

The flame configuration to be analyzed is shown schematically in Fig. 1. The turbulent air flows through a sudden dump configuration for flame stabilization and some means of mixing downstream of the fuel grain in order to burn all of the available fuel in gas phase. The flame is observed to be quite broad near the flow reattachment position and subsequently develops into a turbulent diffusion flame within the boundary layer in the downstream of the reattachment. In this study, we apply the low-Reynolds-number K-ϵ model to solve the turbulent diffusion flame boundary-layer problem. As to combustion, it is modified from the mixing-layer formulation using the infinite fast chemical kinetics and the probability density function (p.d.f.) of the mixture fraction. The applications of four different probability density functions in the combustion model are studied parametrically. After that, the comparisons of detailed flame structures governed by each p.d.f. are given.

Mathematical Model

To begin this work, several assumptions are made for the development of the time-averaged governing equations: The diffusion flame is in a flat-plate boundary layer. The solid is pure fuel and its pyrolysis occurs at constant temperature. The chemical reaction is one-step and infinite fast. All species in the combustion zone are homogeneous in gas phase, and the perfect gas law is obeyed. The values of specific heat, molecular weight, and transport coefficient for each species in the mixture are assumed equal and constant and the turbulent Lewis number is equal to unity.

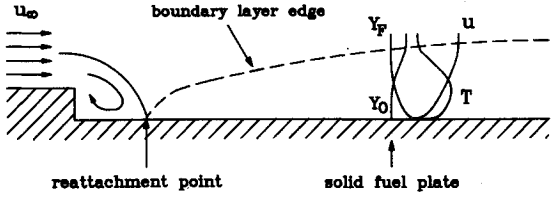

Fig. 1 A conceived solid-fuel plate combustion.

With these assumptions, the time-averaged governing differential equations for two-dimensional boundary layer flow are[9]

Continuity equation:

$$\frac{\partial}{\partial x}(\bar{\rho}\,\bar{u}) + \frac{\partial}{\partial Y}(\overline{\rho v}) = 0 \tag{1}$$

X-Momentum Equation:

$$\bar{\rho}\bar{u}\frac{\partial \bar{u}}{\partial x} + \overline{\rho v}\frac{\partial \bar{u}}{\partial y} = \frac{\partial}{\partial y}\left[(\mu + \mu_t)\frac{\partial \bar{u}}{\partial y}\right] \tag{2}$$

where μ_t is the turbulent viscosity, and is given by [6,7]

$$\mu_t = C_\mu \exp\left[\frac{-2.5}{1 + R_t/50}\right]\bar{\rho}\,K^2/\epsilon \tag{3}$$

where R_t is the turbulent Reynolds number, defined as $K^2\bar{\rho}/\epsilon\mu$. It can be seen that the flow becomes laminar if R_t approaches to zero. On the other hand, turbulent flow is retained when R_t is much greater than unity.

The relative transport equations for solving K and ϵ are given as follows:

$$\bar{\rho}\bar{u}\frac{\partial K}{\partial x} + \overline{\rho v}\frac{\partial K}{\partial y} = \frac{\partial}{\partial y}\left[\left(\mu + \frac{\mu_t}{\sigma_K}\right)\frac{\partial K}{\partial y}\right] + \mu_t\left(\frac{\partial \bar{u}}{\partial y}\right)^2 - \bar{\rho}\epsilon - 2\mu\left(\frac{\partial K^{1/2}}{\partial y}\right)^2 \tag{4}$$

$$\bar{\rho}\bar{u}\frac{\partial \epsilon}{\partial x} + \overline{\rho v}\frac{\partial \epsilon}{\partial y} = \frac{\partial}{\partial y}\left[\left(\mu + \frac{\mu_t}{\sigma_\epsilon}\right)\frac{\partial \epsilon}{\partial y}\right] + C_1\mu_t\frac{\epsilon}{K}\left(\frac{\partial \bar{u}}{\partial y}\right)^2 - C_2\frac{\bar{\rho}\,\epsilon^2}{K} + 2.0\frac{\mu\mu_t}{\bar{\rho}}\left(\frac{\partial^2 \bar{u}}{\partial y^2}\right)^2 \tag{5}$$

Unlike the common-used K-ϵ model, there are several additional terms appearing in Eqs. (4) and (5). The purpose is letting ϵ become zero at the wall for the computational advantage. The correct boundary condition for ϵ at the wall should be

$$\epsilon\Big|_{y=0} = 2\nu\left(\frac{\partial\sqrt{K}}{\partial y}\right)^2\Bigg|_{y=0} \tag{6}$$

It appears to be much more difficult to handle computationally. Jones and Launder suggested to use $\epsilon = 0$ at wall instead by adding the last term to Eq. (4).[6,7]

For a reacting flow subjected to large temperature change, density is affected by the temperature variation through

$$\rho \approx \frac{1}{\bar{T}} \tag{7}$$

which is served as the coupling between momentum and energy equations. The change of molecular viscosity with temperature is taken as

$$\mu \approx \bar{T} \tag{8}$$

The instantaneous species conservation equations for the fuel and oxidizer can be expressed in general form:

$$\rho\frac{\partial Y_i}{\partial t} + \rho u\frac{\partial Y_i}{\partial x} + \rho v\frac{\partial Y_i}{\partial y} = \frac{\partial}{\partial y}\left(\rho D\frac{\partial Y_i}{\partial y}\right) + \dot{\omega}_i, \quad i = \mathrm{F}, \mathrm{O} \tag{9}$$

where ω_i is the species-production term. There has not been significant development in the use of moment methods modeling the unclosed species-production-rate term $\dot{\omega}_i$. For the diffusion flame, this problem can be circumvented if the reaction time is negligibly short in comparison with the mixing time. This assumption implies that the instantaneous molecular-species concentrations and temperature only are functions of conserved scalar at that instant.[10] Since the molecular-species concentrations are directly related to the conserved scalar and the statistics of all thermodynamic variables are obtainable from the knowledge of the statistics of the scalar, a typical choice for the strictly conserved scalar variable is the mixture fraction, f, which has been applied successfully to diffusion flame boundary-layer problems.[10,11]

The mixture fraction f in the present problem is defined as

$$f = \frac{\phi - \phi_\infty}{\phi_w - \phi_\infty} \tag{10}$$

where $\phi = Y_F - Y_O/i$, i is the stoichiometric mass ratio of oxidizer to fuel, subscript ∞ indicates the edge of the boundary layer, and w represents the solid fuel surface. A stoichiometric mixture fraction can be found by setting $\phi = 0$, i.e.,

$$f_{st} = \frac{-\phi_\infty}{\phi_w - \phi_\infty} = \frac{Y_{O\infty}/i}{Y_{fw} + Y_{o\infty}/^i} \tag{11}$$

From Eqs. (10) and (11), the instantaneous relationship between Y_F, Y_O, and f becomes

$$0 \le f < f_{st}, \qquad Y_F = 0, \qquad Y_O = Y_{O\infty}\left(1 - \frac{f}{f_{st}}\right)$$

$$f_{st} < f \le 1, \qquad Y_F = Y_{Fw}\left(\frac{f - f_{st}}{1 - f_{st}}\right), \qquad Y_O = 0 \tag{12}$$

Since the diffusion coefficients for fuel and oxidizer are assumed equal in Eq. (9), the resulting time-averaged equation for mixture fraction becomes

$$\bar{\rho}\bar{u}\frac{\partial \bar{f}}{\partial x} + \bar{\rho}\bar{v}\frac{\partial \bar{f}}{\partial y} = \frac{\partial}{\partial y}\left[\left(\frac{\mu}{P_r} + \frac{\mu_t}{P_t}\right)\frac{\partial \bar{f}}{\partial y}\right] - \bar{\rho}\bar{u}\cdot\frac{\bar{f}}{\phi_w - \phi_\infty}\cdot\frac{\partial \bar{\phi}_w}{\partial x} \tag{13}$$

Later we shall see that the solution of Eq. (13) alone is not enough to solve the two unknown time-average quantities $\bar{Y}_F$ and $\bar{Y}_O$ by the use of probability density function. An additional transport equation, termed the g-equation, is introduced to find $\bar{Y}_F$ and $\bar{Y}_O$. g is defined as the square of the mixture-fraction fluctuation, namely $\overline{f'^2}$. The governing equation for g, which resembles the K-equation, [11] is

$$\bar{\rho}\bar{u}\frac{\partial g}{\partial x} + \overline{\rho v}\frac{\partial g}{\partial y} = \frac{\partial}{\partial y}\left[\left(\frac{\mu}{P_r} + \frac{\mu_t}{P_t}\right)\frac{\partial g}{\partial y}\right] + C_{g1}\mu_t\left(\frac{\partial \bar{f}}{\partial y}\right)^2 - C_{g2}\,\rho\frac{\epsilon}{K}g \tag{14}$$

Because of the use of mixture fraction and probability density function, it is not necessary to solve Eq. (9) directly to obtain Y_F and Y_O. The time-averaged mass fractions of $\bar{Y}_F$ and $\bar{Y}O$ are related by probability density function $p(f)$ in the following way.

$$\bar{Y}_O = \int_0^1 Y_O(f)\,p(f)\,df$$

$$\bar{Y}_F = \int_0^1 Y_F(f)\,p(f)\,df \tag{15}$$

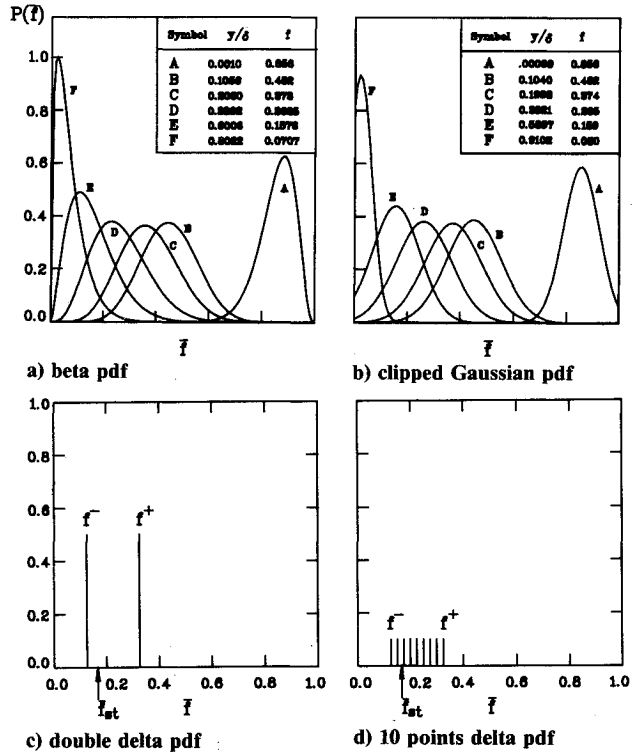

Fig. 2 Distributions of beta, clipped Gaussian, double delta (at $\bar{f}=0.2213$, $g=1.0072337\times10^{-2}$), and ten-point delta (at $\bar{f}=0.2213$, $g=1.0072337\times10^{-2}$) probability density functions across the boundary layer.

In this study, four types of p.d.f.s are adopted. They are the beta probability density function, clipped Gaussian probability density function double delta probability density function, and the ten-point delta probability density function, respectively, which are described in detail as follows:

1) Beta Probability Density Function (β – p.d.f.):

The beta probability density function, illustrated graphically in Fig. 2A, is written as[8,12,13]

$$p(f) = \frac{f^{\alpha-1}(1-f)^{\beta-1}}{\int_0^1 f^{\alpha-1}(1-f)^{\beta-1}df} \qquad 0 \le f \le 1 \tag{16}$$

where the two parameters α and β are determined explicitly by

$$\alpha = (\bar{f} - \bar{f}^2 - g) - \frac{\bar{f}}{g}$$

$$\beta = (\bar{f} - \bar{f}^2 - g)\frac{1-\bar{f}}{g} \tag{17}$$

As soon as the values of $\bar{f}$ and g are know via Eqs. (13) and (14), α and β are solved at each grid point by the above equations and the p.d.f. is determined at that point by using Eq. (16). Then $\bar{Y}_F$ and $\bar{Y}_O$ can be evaluated by Eq. (15).

2) Clipped Gaussian Probability Density Function (C-p.d.f.):

This function is in form of [14]

$$p(f) = -\frac{1}{\sigma\sqrt{2\pi}}\exp\left[-\frac{1}{2}\left(\frac{f-\mu}{\sigma}\right)^2\right][H(f) - (f-1)] + A\,\delta(0) + B\,\delta(1)$$

where

$$A = \int_{-\infty}^{0} -\frac{1}{\sigma\sqrt{2\pi}}\exp\left[-\frac{1}{2}\left(\frac{f-\mu}{\sigma}\right)^2\right]df \tag{18a}$$

$$B = \int_1^\infty -\frac{1}{\sigma\sqrt{2\pi}} \exp\left[-\frac{1}{2}\left(\frac{f-\mu}{\sigma}\right)^2\right] df \tag{18b}$$

$H(\phi)$ is the Heaviside unit step function, $\delta(\phi)$ is the delta function, μ is the maximum probability, and σ is the variance. The profile is expressed by the Gaussian distribution within the range $0 < f < 1$, but the sidetails of the distribution are replaced by δ functions at $f = 0$ and 1, respectively. Figure 2B shows the clipped Gaussian configuration. The most probable values of distribution μ and variance σ are determined by the values of $\bar{f}$ and g, which are:

$$\bar{f} = \int_0^1 fp(f)df$$

$$g = \overline{f'^2} = \int_0^1 (f-\bar{f})^2 p(f)df \tag{19}$$

From above equations, we can obtain the values of μ and σ iteratively for which the detailed procedure can be referred in Ref. 19. Substituting them into Eq. (18), we can have $\bar{Y}_F$ and $\bar{Y}_O$ by using Eq. (15).

3) Double Delta Probability Density Function and Ten-Point Delta Probability Density Function:

The double delta p.d.f., proposed by Khalil et al.,[15] is presented by a rectangular-wave variation (See Fig. 2C):

$$p(f) = a\delta(f-f^+) + (1-a)\,\delta(f-f^-) \tag{20}$$

where $f^+ = f + g^{1/2}$, $f^- = f - g^{1/2}$, and a is equal to 0.5. The parameter a is the probability at that point.

The double delta p.d.f. was stated by Jones[16] that its results are unsatisfactory in comparison with Kent and Bilger's measurements.[17] According to Kent and Bilger,[18] we adopt a modified delta p.d.f. by extending the two-point delta function to a ten-point delta function, where it can be seen in Fig. 2D. The interval (f^+, f^-) is divided into nine sections and consequently the parameter a becomes 0.1.

The functions presented above are widely used to describe the probability distribution of $\bar{f}$ ranged between 0 and 1 in turbulent flames. However, these studies, cited in each category of p.d.f.s are concerned with the combustion problems of gaseous fuels except that in Ref. 8. The present study motivated from the last work is to apply these four p.d.f.s to solid fuel combustion and subsequently to investigate their effects on the flame structures.

The time-averaged energy conservation equation is given by

$$\bar{\rho}\bar{u}\frac{\partial C_p\bar{T}}{\partial x} + \bar{\rho}\bar{v}\frac{\partial C_p\bar{T}}{\partial y} = \frac{\partial}{\partial y}\left[\left(\frac{\mu}{P_r} + \frac{\mu_t}{P_t}\right)\frac{\partial C_p\bar{T}}{\partial y}\right] - \bar{\omega}_F q \tag{21}$$

where q is the heat of combustion per unit mass of fuel consumed. Similarly, we also have the same closure difficulty with the average reaction rate $\bar{\omega}_F$. Therefore, a conserved variable $\bar{H}$ is used instead, defined as

$$\bar{H} = C_p\bar{T} + \bar{Y}_O q/i \tag{22}$$

Combining the time-averaged oxidizer species equation in Eq. (9) with Eq. (21) yields

$$\bar{\rho}\bar{u}\frac{\partial \bar{H}}{\partial x} + \bar{\rho}\bar{v}\frac{\partial \bar{H}}{\partial y} = \frac{\partial}{\partial y}\left[\left(\frac{\mu}{P_r} + \frac{\mu_t}{P_t}\right)\frac{\partial \bar{H}}{\partial y}\right] \tag{23}$$

Finally, in order to complete the mathematical description, the boundary conditions must be specified. They are described as follows:

At the edge of the boundary layer ($y \to \infty$):

$$\bar{u} = u_\infty, \quad \frac{\partial K}{\partial y} = 0, \quad \frac{\partial \epsilon}{\partial y} = 0, \quad \bar{f} = 0$$

$$g = 0, \quad \bar{H} = C_p\bar{T}_\infty + Y_{O\infty}q/i \tag{24}$$

At the surface of solid fuel ($y = 0$)

$$\bar{u} = 0, \quad \bar{K} = 0, \quad \epsilon = 0, \quad \bar{f} = 1, \quad \bar{H} = \bar{H}_w = C_p\bar{T}_w \tag{25}$$

and the boundary condition of g at $y = 0$ is derived by applying fuel conservation over a control surface which yields

$$g_w = \frac{\bar{\rho}D}{2\bar{m}_b}\cdot\frac{\partial g_w}{\partial y} + \frac{1-\bar{Y}_{Fw}}{\dot{m}_b(Y_{Fw} + Y_{O\infty}/i)^2}\left(-\bar{\rho}D_t\frac{\partial \bar{Y}_F}{\partial y}\right)_w \tag{26}$$

The mass burning rate $\bar{m}_b$ can be obtained by using an energy balance at the solid fuel surface:

$$\bar{m}_b = \frac{(K\frac{\partial \bar{T}}{\partial y})_w}{L + C_s(\bar{T}_w - T_s)} \tag{27}$$

where $\bar{m}_b = (\bar{\rho}\bar{v})_w$. L, C_s, and T_s are the latent heat, the heat capacity, and the bulk temperature of the solid, respectively. On the right-hand side of Eq. (27), the numerator represents the rate of heat conducted to the solid wall from the gas phase and the denominator represents the heat required to transform a unit mass of solid initially at temperature T_s into vapor at temperature $\bar{T}_w$. The boundary value of $\bar{Y}_{Fw}$ is determined by mass balance on the wall, expressed as

$$\bar{m} = \bar{m}\,\bar{Y}_{Fw} + \bar{\rho}D_t\left(\frac{\partial \bar{Y}_F}{\partial y}\right)_w \tag{28}$$

Numerical Calculation

The problem is solved numerically. The development of a numerical scheme from differential equations to difference ones, the treatment of probability density function, and the computational procedure can be found in Ref. 19. In that reference, two limiting cases, the incompressible rigid wall flat-plate turbulent boundary layer and the same flow configuration with uniform mass blowing, are tested in advance to ensure the accuracy of the scheme. The results are in good agreement with that by applying the 1/7 law as well as the data measured by Klebanoff[20] and by Mickley and Davies[21] separately.

Results and Discussion

In this study, polymethylmethacylate (PMMA) is selected as the solid fuel and the freestream fluid is air. The properties of fuel, air, and gas mixture used in this computation are listed in Table 1. Based on the data in Table 1, the adiabatic flame temperature is found to be 2550 K. The various constants, which appear in the governing equations mentioned previously, are listed below in Table 2.[8]

The results presented are picked up at $820\delta_0$, corresponding to 28.7 m downstream of the starting point so that the initial-profile influence is negligible.

The computed results of infinite-fast combustion calculation in different coordinates are shown in Fig. 3. In Fig. 3A, where the abscissa is f, the adiabatic temperature occurs at the mixture fraction in its stoichiometric condition. The temperature and species-concentration are in linear relation because from Eq. (12) Y_F and Y_O are proportional to f. Figure 3B shows the corresponding flame structures across the boundary layer in y/δ coordinate. It can be seen that f_{st} is located at $y/\delta = 0.58$.

The turbulent flame structures in the following figures are presented for each applied probability density function. It can

Table 1 Property values

Name	Symbol	Value	Unit
PMMA molecular weight	M	100	g/g-mole
latent heat	L	1050	kJ/kg
heat of reaction	q	22960	kJkg-fuel
Stoichiometric mass ratio	i	1.92	
fuel surface temperature	T_w	750	K
interior fuel temperature	T_s	300	K
fuel specific heat	C_s	1.463	kJ/kg-K
air temperature	T_∞	1000	K
air density	ρ_∞	0.3532	kg/m^3
molecular viscosity	μ	4.65×10^{-5}	kg/m-s
airstream velocity	u_∞	30	m/s
average specific heat	C_p	1.4542	kJ/kg-K
Prandtl number	P_r	0.9	
turbulent Prandtl number	P_t	0.9	
Lewis number	L_e	1.0	
turbulence Lewis number	L_t	1.0	

Table 2. Fuel, air, and gas mixture properties

C_μ	C_1	C_2	C_{g1}	C_{g2}	σ_ϵ	σ_k	σ_H
0.09	1.55	2.0*	2.7	1.79	1.3	1.0	0.9

*At low turbulence Reynolds number $C_2 = 2.0\ [1.0-0.3\exp(-R_T^2)]$.

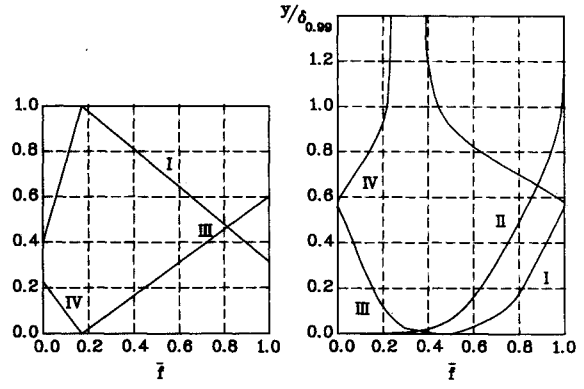

Fig. 3 Flame structures of turbulent diffusion flame under infinite-fast kinetics (I: $\bar{T}/T_{ad}$; II: $\bar{U}/U\infty$; III: $\bar{Y}_F$; IV: $\bar{Y}_O$).

be seen that they are quite similar to each other; therefore, we describe the flame feature in general aspects first and then compare this turbulent flame influenced by the imposition of p.d.f. with that by the infinite-fast kinetics assumption just mentioned. The discrepancy between the flames due to the different application of p.d.f.s is also discussed figure by figure.

Figure 4 shows the calculated distributions of species mass fractions and temperature plotted against the mixture fraction $\bar{f}$. The highest temperature is found to occur at the rich side of the stoichiometric condition. The mass fractions of oxidizer and fuel fall from their maximum values at $\bar{f}=0$ and $\bar{f}=1$, respectively, to the stoichiometric condition at $\bar{f}=0.1667$. At the stoichiometric point, both $\bar{Y}_O$ and $\bar{Y}_F$ are nonzero which is unlike that in infinite-fast combustion shown in Fig. 3. This is consistent with the measurement of Razdan and Stevens.[4] It is the so-called "unmixedness" phenomenom that delays the combustion of even highly reactive fuels in turbulent diffusion flames. In these flames, the reaction is spread over regions of substantial thickness, in which both fuel and oxidizer have significant concentrations. Despite these concentrations and the high chemical reactivity, the reaction proceeds slowly because the fuel and oxidant are presented at a given point at different times.[11]

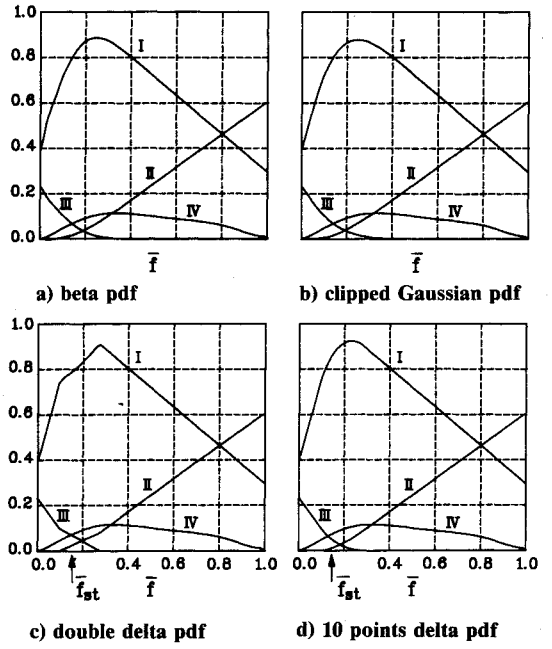

Fig. 4 $\bar{T}/T_{ad}$(I), $\bar{Y}_F$(II), $\bar{Y}_O$(III) and g(IV) distributions vs mixture fraction $\bar{f}$.

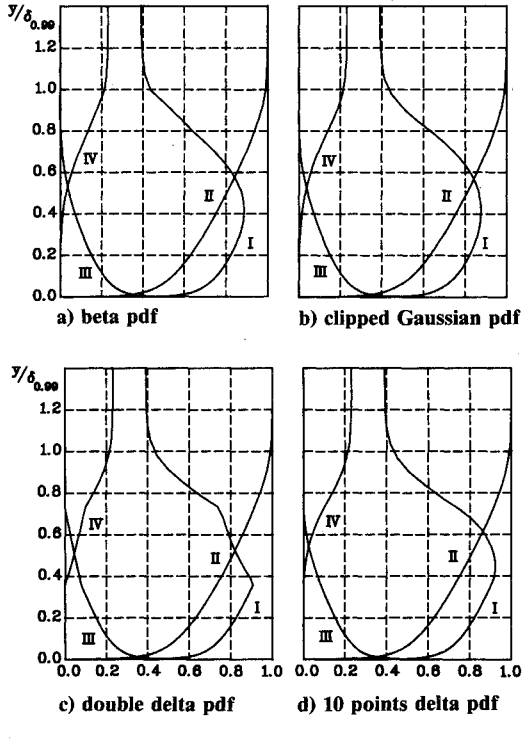

Fig. 5 $\bar{T}/T_{ad}$(I), $\bar{u}/u_\infty$(II), $\bar{Y}_F$(III), and $\bar{Y}_O$(IV) distributions in turbulent diffusion flame boundary layer.

Another view of the turbulent flame structure across the solid-fuel boundary layer is shown in Fig. 5 where the abscissa is y/δ instead of $\bar{f}$. The peak temperature is lower than the adiabatic one owing to the introducing of the probability density function. Fuel and oxidizer are overlapped near the peak temperature region. It is shown that the broader the overlapped region, the lower the peak temperature. The mean temperature profile is much more rounded in the peak region compared with those found in laminar flames due to the turbulent fluctuation.

It can be seen that in the clipped Gaussian and beta p.d.f.s, the species mass-fraction profiles are identical and the temper-

atures profiles are almost the same with the maximum temperature difference being less than 1%. For both p.d.f.s, the peak temperature is about 88% of the adiabatic flame temperature which occurs at $y/\delta = 0.41$. Consistently, there is a substantial overlap of the averaged fuel and oxidizer mass fractions for $0.2 < y/\delta < 0.8$. The temperature profile of the double delta p.d.f. shows that there exists two discontinuities between the species overlapping region, which is also mentioned in Ref. 22. The reason will be explained later. Outside the region, the temperature profile is similar to that by the infinite-fast kinetic assumption (see Fig. 3). The predicted highest temperature is 2.1% greater than that of beta p.d.f. The temperature profile of the 10-point delta p.d.f. appears to be rounded again, and its peak value is 92% of the adiabatic one and is higher than that of the others since it has the smallest overlapping region.

Figures 6 and 7 show the molecular viscosity and eddy viscosity distributions inside the boundary layer. In Fig. 6, we can see that μ_t is much greater than μ, indicating that it is a fully turbulent region there. The molecular viscosity profile is similar to temperature profile since it can be detected from Eq. (8), where $\mu \approx \bar{T}$. However, it shows that μ_t is not always greater than μ close to the wall in Fig. 7. This explains the necessity of the near-wall manipulation. The point where $\mu_t = \mu$ is at $y/\delta = 1.01 \times 10^{-3}$ ($y^+ = 3$). In this study, the first grid point is located at $y^+ = 0.18$ such that the computing domain includes the viscous sublayer. Other authors select the point inside the domain, from $y^+ = 30$ to 50, to patch the laminar and turbulent regions in the wall-function method. It

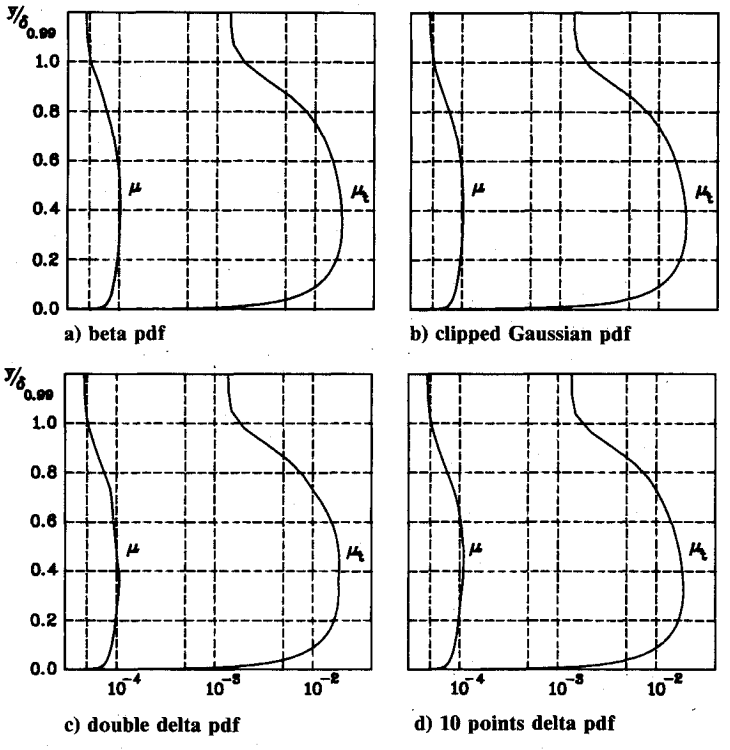

Fig. 6 Molecular viscosity and turbulent viscosity distribution in turbulent diffusion flame boundary layer.

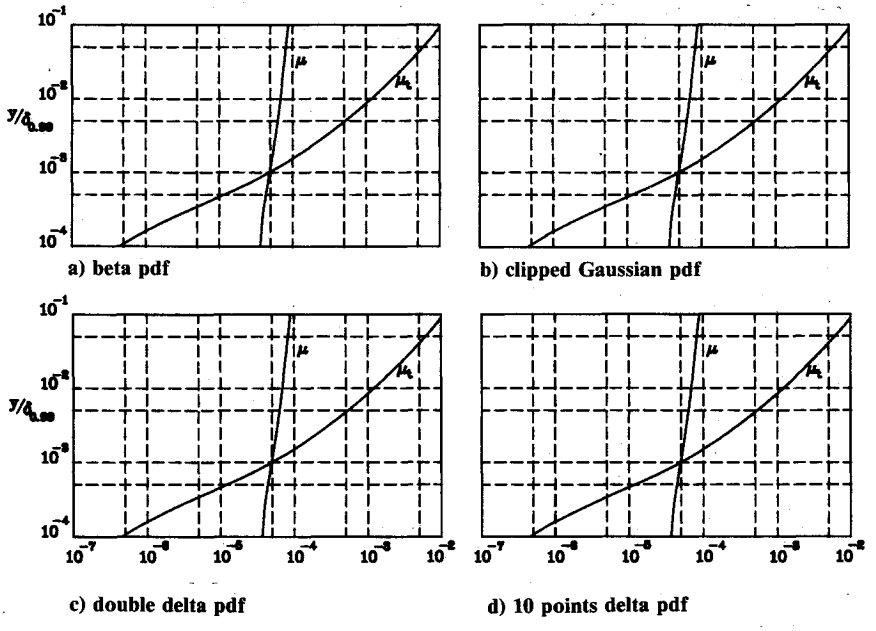

Fig. 7 Molecular viscosity and turbulent viscosity distribution near the wall in turbulent diffusion flame boundary layer.

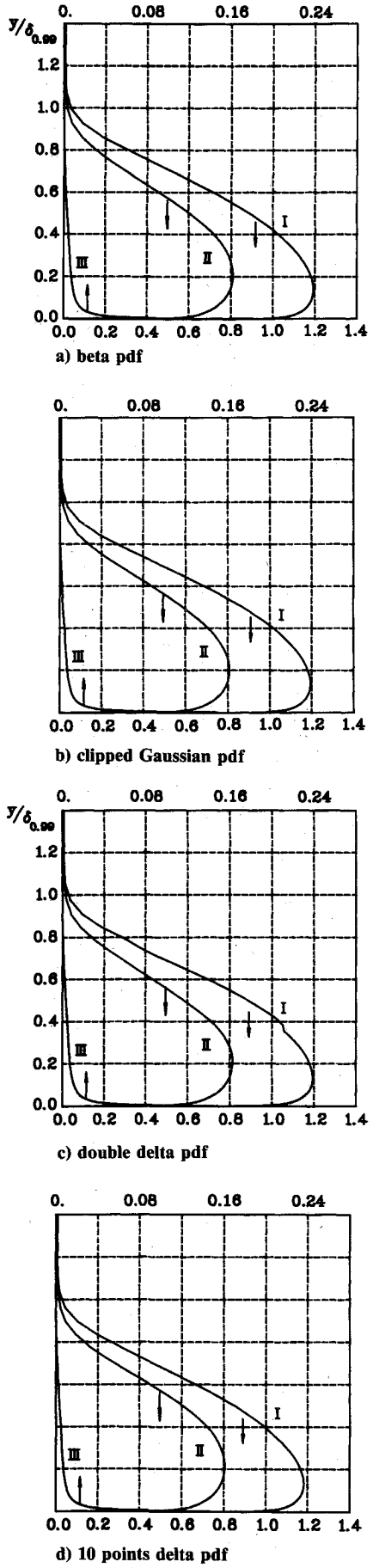

Fig. 8 Dimensionless turbulent kinetic enrgy K^*, shear stress τ^*, and dissipation rate ϵ^* in turbulent boundary layer (I: $\tau^* \times 1000$; II: $K^* \times 100$; III: $\epsilon^* \times 10^{-6}$).

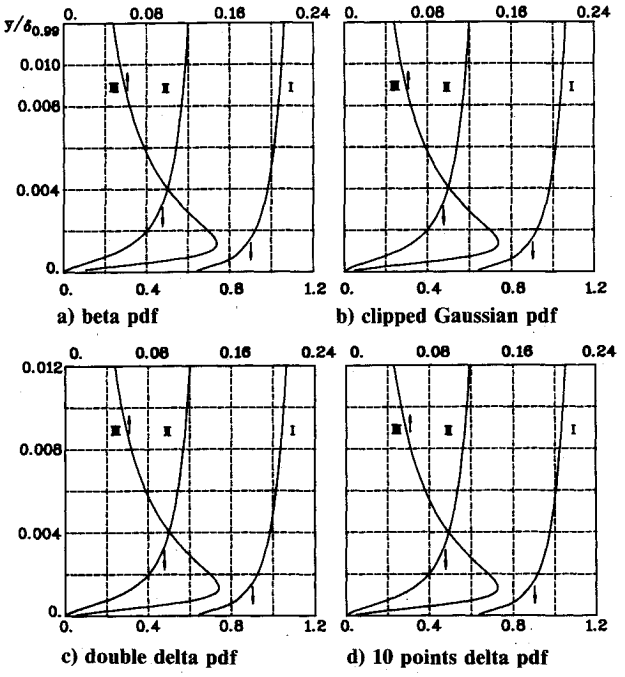

Fig. 9 Dimensionless turbulent kinetic energy K^*, shear stress τ^*, and dissipation rate ϵ^* near the wall in turbulent boundary layer (I: $\tau^* \times 1000$; II: $K^* \times 100$; III: $\epsilon^* \times 10^{-6}$).

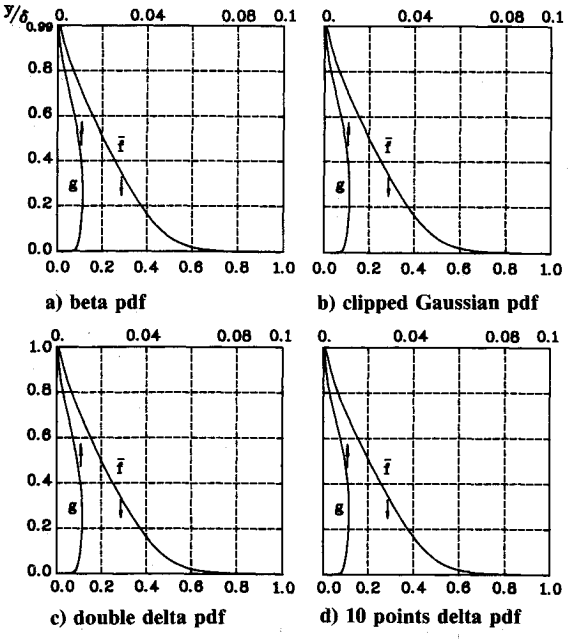

Fig. 10 $\bar{f}$ and g distribution inside the turbulent boundary layer.

is between $\mu = 0.03\mu_t$ and $0.05\mu_t$, corresponding to where the fully turbulent hypothesis is applied.

The dimensionless turbulence kinetic energy k^*, dissipation rate ϵ, and shear stress τ^* distributions are shown in Figs. 8 and 9. The location of the maximum shear stress shifted away from the wall in Fig. 8, which is caused by the coupling of turbulent viscosity and velocity gradient. Also, the position of maximum turbulent kinetic energy is raised up and is at a large distance from the wall, which is quite different from the incompressible case. The phenomenon was also observed by Razdan and Kuo.[23] However, the peak of dissipation rate stays close to the wall.

The differences for the τ^*, k^*, and ϵ^* distributions among the applied p.d.f.s are very small. The shear stress in the

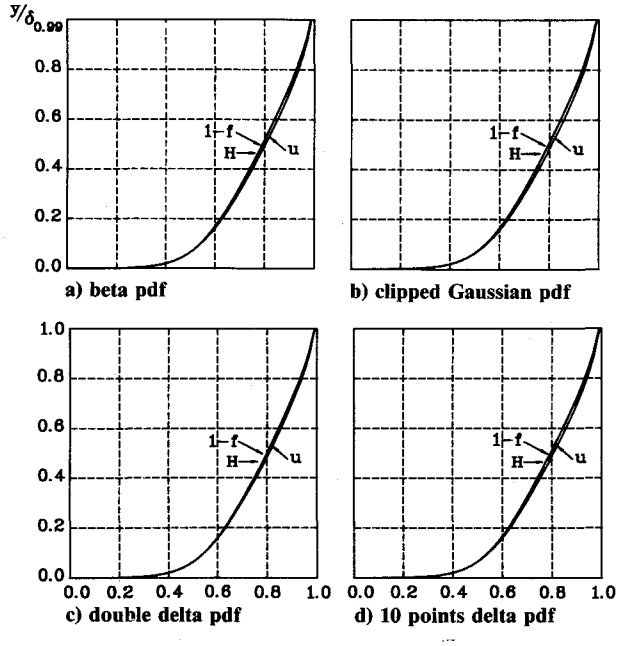

Fig. 11 Dimensionless velocity, mixture-fraction, and enthalpy distributions inside the turbulent boundary layer.

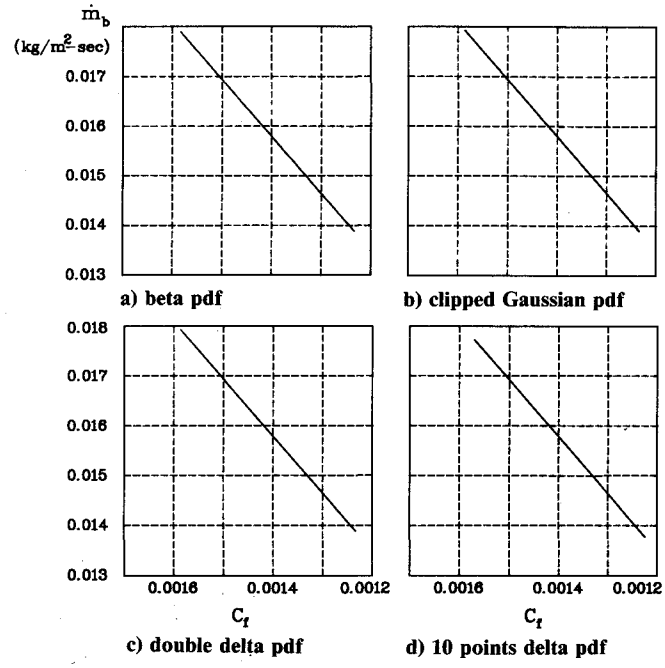

Fig. 12 Mass burning rate vs skin friction.

double delta p.d.f. has a discontinuity at $y/\delta_{0.99} = 0.39$. This is due to the temperature (viscosity) discontinuity there.

The distribution of mean square of mixture-fraction fluctuation g and mixture fraction f are shown in Fig. 10. The fluctuation is strong inside $0.01 < y/\delta < 0.5$, which is due to the coupling of temperature fluctuation and velocity gradient.

The profiles of nondimensional velocity $\hat{u}$, enthalpy $\hat{H}$, and mixture fraction $\tilde{f}$ are shown in Fig. 11, where $\hat{u} = (u/u_\infty)$ and $\hat{H} = (H - H_w)/(H_\infty - H_w)$. It is found that the profiles are similar to each other, indicating that the generalized Reynolds analogy is valid even near the hot combustion region. It is also found in Ref. 2. It may be intuitively expected that the presence of combustion within a boundary layer will alter the momentum transfer across the boundary layer. It appears that the heat release should further reduce the velocity gradient through density reduction mentioned by Wooldridge.[2] In our study, no velocity inflection occurs near the flame sheet since there is no pressure gradient in the streamwise direction for flat-plate boundary-layer combustion. The velocity profile is much fuller than that in the laminar boundary-layer flame due to the appearance of Reynolds stress.

Figure 12 shows the relationship between mass burning rate and friction coefficient. The friction coefficient decreases downstream which resembles the trend of the mass burning rate. The ratio $\bar{m}_b/C_f$ is found to be constant over the range of computation. This result indicates that the burning rate in the flat-plate turbulent boundary-layer flame is proportional to the friction coefficient (or velocity gradient) at the surface. A similar conclusion is also found in the laminar boundary-layer flame, such as the classical problem by Emmons.[24]

So far, we have mentioned some differences among these flame structures figure by figure due to the different application of p.d.f.s, the basic differences among these p.d.f.s, and the reasons causing the discrepancies between the resulted flame structures are discussed as follows.

Figure 2A and 2B show the beta p.d.f. (β – p.d.f.) and clipped Gaussian p.d.f. (C – p.d.f.) distributions separately. The two profiles are similar in the same location. This is why the profiles of the temperature and species concentrations have a little differences in applying these two p.d.f.s. The major differences are at the boundary ($\tilde{f} = 0$ and $\tilde{f} = 1$). In the β – p.d.f. [see Eq. (16)], $p(f)$ becomes zero on both ends whereas the corresponding values in the C – p.d.f. are not [see Eq. (19)]. In the latter case, the probabilities outside these two boundaries are lumped into the outer bounds.

The double delta p.d.f. distribution can be seen in Fig. 2C. It is made of two delta functions at the specified positions rather than a smooth curve over the domain as the beta p.d.f. or the clipped Gaussian p.d.f. For $\tilde{f}_{st}$ outside the domain between f^- and f^+, the reaction rate is treated as infinite fast. Otherwise, ($f^- < \tilde{f}_{st} < f^+$):

$$p(f) = 0.5 \cdot \delta(f - f^+) + 0.5 \cdot \delta(f - f^-)$$

When $\tilde{f}_{st}$ is very close to f^-, which indicates the probability of Y_F should be dominant. However, from above expression the probabilities of Y_O and Y_F are equal which is unrealistic. Therefore, the discontinuities result as $\tilde{f}_{st}$ is approached to f^- or f^+.

A modified p.d.f. is shown in Fig. 2D. The two-delta function in f is replaced by a ten-delta function, where the domain is arranged into nine equal-spaced subdivisions. It avoids the incorrect situations near f^- and f^+ mentioned above and eliminates the discontinuities.

Both double delta p.d.f. and ten-point delta p.d.f. are not correct from the viewpoint of statistics. For example, in Fig. 2C, f^-, which is starting point of the overlapping region, is equal to σ. It means that the probability outside f^-, which includes the 15.87% probabilities, does not count in the function. The same error also occurs at the right-hand side of f^+. Further improvements are needed in applying these two p.d.f. methods.

Conclusions

A combustion model for turbulent flame adjacent to a solid-fuel plate in a parallel oxidizer flow is established. The flow is assumed to be boundary layer and the mean properties of the turbulent flowfield are calculated by the use of low-Reynolds-number K-ϵ model. The instantaneous thin-flame theory together with the probability density function are used in the combustion model. The temperature is determined as soon as the distributions of averaged fuel and oxidizer mass fractions, via the integration of the product of their instantaneous quantities and p.d.f. over the corresponding domain, are obtained.

There are four kinds of p.d.f's adopted in this study. They are the beta p.d.f., the clipped Gaussian p.d.f., the double delta p.d.f., and the ten-point delta p.d.f., respectively.

By application of the p.d.f., the time-averaged mass fraction of fuel and oxidizer overlap substantially. This is the

so-called "unmixedness" phenomenon that reduces the highest temperature at the reaction zone and forms a rounded temperature profile. The mean temperature profile and its maximum depend on the distributions of $\bar{Y}_F$ and $\bar{Y}_O$ and the depth of their overlap, which are influenced by the form of p.d.f. However, it is found that the velocity, mixture fraction and its fluctuation, and total enthalpy are similar no matter what kind of p.d.f. is applied.

The flame structures are identical for the application of the beta p.d.f. and the clipped Gaussian p.d.f. because their appearances are almost the same except on both endpoints. The profiles show the occurrence of discontinuity by the use of the double delta p.d.f. due to the unreasonable distribution proportion. A modified ten-point delta p.d.f. is used and the discontinuity no longer existed. However, it results in the smallest overlap between $\bar{Y}_F$ and $\bar{Y}_O$ where the flame temperature is the highest.

As with most turbulent modeling the ultimate check of success lies on its comparison with experiment. Unfortunately, as noted in the review,[25] there is a lack of detailed data on solid-fuel turbulent reacting flow, which is obviously an area where more work is needed.

Acknowledgment

The authors acknowledge the support of National Research Council of Taiwan, Republic of China, under Grant NSC78-0401-E009-006.

References

[1]Marxman, G. A., "Combustion in the Turbulent Boundary on a Vaporizing Surface," *Tenth Symposium (International) on Combustion,* Cambridge, England, 1965, pp. 1337–1349.

[2]Wooldridge, G. E., and Muzzy, R. J., "Measurements in a Turbulent Boundary Layer with Porous Wall Injection and Combustion," *Tenth Symposium (International) on Combustion,* Cambridge, England, 1965, pp. 1351–1362.

[3]Netzer, D. W., "Modeling Solid-Fuel Ramjet Combustion," *Journal of Spacecraft,* Vol. 14, No. 12, 1977, pp. 762–766.

[4]Razdan, M. K., and Stevens, J. G., "CO/Air Turbulent Diffusion Flame: Measurements and Modeling," *Combustion and Flame,* Vol. 59, March 1985, pp. 289–301.

[5]Most, J. M., Harivl, N., Joulain, P., Ruttun, B., and Sztal, B., "Influence of Turbulent Diffusion Flame on Transport Phenomena to a Reacting Surface," *19th Symposium (International) on Combustion,* Haifa, Israel, 1982, pp. 375–386.

[6]Jones, W. P., and Launder, B. E., "The Prediction of Laminarization with a Two-Equation Model of Turbulence," *International Journal of Heat and Mass Transfer,* Vol. 15, Feb. 1972, pp. 301–314.

[7]Jones, W. P., and Launder, B. E., "The Calculation of Low-Reynolds-Number Phenomena with a Two-Equation Model of Turbulence," *International Journal of Heat and Mass Transfer*, Vol. 16, June 1973, pp. 1119–1130.

[8]Shan, D. Y-Y., and T'ien, J. S.,"Application of Low-Reynolds-number K-ϵ Model on Solid-Fuel Turbulent Boundary-Layer Combustion," AIAA Paper 87-1778, June 1987.

[9]Cebeci, T., and Smith, A. M. O., The Boundary-Layer Equations, *Analysis of Turbulent Boundary Layers—Applied Mathematics and Mechanics,* An International Series of Monographs, Academic, Orlando, FL, 1974, pp. 62–90.

[10]Bilger, R. W., Turbulent Flows with Nonpremixed Reactants, *Turbulent Reacting Flows—Topics in Applied Physics,* Springer-Velag, New York, 1980, pp. 65–114.

[11]Spalding, D.B., "Concentration Fluctuations in a Round Turbulent Free Jet.," *Chemical Engineering Science,* Vol. 26, Feb. 1971, pp. 95–107.

[12]Vanka, S. P., "Calculation of Axisymmetric, Turbulent, Confined Diffusion Flames," *AIAA Journal,* Vol. 24, No. 3, 1986, pp. 462–499.

[13]Jones, W. P., and Preddin, C. H., "Predictions of the Flowfield and Local Gas Composition in Gas Turbine Combustors" *17th Symposium (International) on Combustion,* Leeds, England, 1978, pp. 399–409.

[14]Lockwood, F. C., and Naguib A. S., "The Prediction of the Fluctuations in the Properties of Free, Round-Jet, Turbulent, Diffusion Flames," *Combustion and Flame,* Vol. 24, July 1975, pp. 109–124.

[15]Khalil, E. E., Spalding, D. B., and Whitelaw, J. H., "The Calculation of Local Flow Properties in Two-Dimensional Furnaces," *International Journal of Heat and Mass Transfer,* Vol. 18, June 1975, pp. 775–791.

[16]Jones, W. P., "Models for Turbulent Flows with Variable Density," *VKI Lecture Series 1979-2, Prediction Methods for Turbulent Flows,* Hemisphere, New York, 1980, pp. 380–421.

[17]Kent, J. H., and Bilger, R. W., "Turbulent Diffusion Flames," *14th Symposium (International) on Combustion*, University Park, PA, 1973, pp. 615–626.

[18]Kent, J. H., and Bilger, R. W., "The Prediction of Turbulent Diffusion Flame Fields and Nitric Oxide Formation," *16th Symposium (International) on Combustion,* University Park, PA, 1976, pp. 1643–1656.

[19]Lan, C. Y., "Turbulent Boundary-Layer Diffusion Flame: Effects of Probability Density Function," M.S. Thesis, National Chiao Tung Univ., Taiwan, R.O.C., June 1989.

[20]Klebanoff, P. S., "Characteristics of Turbulence in Boundary Layer with Zero Pressure Gradient," NACA Rept. 1247, 1955.

[21]Mickley, H. S., and Davis, R. S., "Momentum Transfer for Flows Over a Flat Plate with Blowing," NACA TN 4017, 1957.

[22]Bradshaw, P., Cebeci, T., and Whitelaw, J. H., Combustion, *Engineering Calculation Methods for Turbulent Flow,* Springer-Verlag, Academic, New York, 1981, pp. 290–309.

[23]Razdan, B. F., and Kuo, K. K., "Turbulent Flow Analysis of Erosive Burning Cylindrical Composite Solid Propellants," *AIAA Journal*, Vol. 20, Jan. 1982, pp. 122–128.

[24]Emmons, H., "The Film Combustion of Liquid Fuel," *Zeitschrift fuer Agnew, Mathematische Mechanik*, Bd. 36, Jan.-Feb. 1956, pp. 60–71.

[25]Strahle, W. C., and Lekoudis, S. G. (ed.), "Evaluation of Data on Simple Turbulent Reacting Flows, Air Force Office of Scientific Research, AFOSR TR-85-0880, March 1985.